Mode set focused hybrid estimation

Theresa Rienmüller, Michael Hofbaur, Louise Travé-Massuyès, Mehdi Bayoudh

MODE SET FOCUSED HYBRID ESTIMATION

THERESA RIENMÜLLER [*,**], MICHAEL HOFBAUR [***], LOUISE TRAVÉ-MASSUYÈS [****], MEHDI BAYOUDH [****]

[*] Institute of Electrical and Biomedical Engineering
UMIT, Eduard-Wallnöfer-Zentrum 1, 6060 Hall in Tyrol, Austria
email: theresa.rienmueller@umit.at

[**]Doctoral School of Information and Communications Engineering (ICE)
Graz University of Technology, Rechbauerstrasse 12, 8010 Graz, Austria

[***]Institute of Automation and Control Engineering
UMIT, Eduard-Wallnöfer-Zentrum 1, 6060 Hall in Tyrol, Austria
email: michael.hofbaur@umit.at

[****]LAAS, CNRS
University of Toulouse, 7 Avenue du Colonel Roche, F-31400 Toulouse, France
email: {louise,bayoudh}@laas.fr

Estimating the state of a hybrid system means accounting for the mode of operation or failure and the current state of the continuously valued entities concurrently. Existing hybrid estimation schemes try to overcome the problem of an exponentially growing number of possible mode-sequence/continuous-state combinations by merging hypotheses and/or deducing likelihood measures to identify tractable sets of the most likely hypotheses. However, they still suffer from unnecessarily high computational costs as the number of possible modes increases. Hybrid diagnosis schemes, on the other hand, estimate the current mode of operation/failure only, thus leaving the continuous evolution of the system implicit. This paper proposes a novel scheme that uses a combination of both the approaches in order to define posterior transition probabilities between the specified modes of the hybrid system, hence focusing better on relevant hypotheses. In order to demonstrate the effectiveness of the proposed method, the algorithm is applied to a satellite attitude control system and compared with existing hybrid estimation/diagnosis schemes, such as the Interacting Multiple Model (IMM) algorithm, a purely parity based method (HyDiag), and an existing hybrid Mode Estimation (hME) algorithm.

Keywords: hybrid systems, fault detection and diagnosis, monitoring and estimation.

1. Introduction

Many modern systems, such as immobile and mobile robots, space probes, etc. show complex behaviour with several modes of operation or failure, each of them associated with different continuous dynamics. Accurate knowledge of the current mode and the current state of the physical entities is important for autonomous operation in order to react appropriately whenever faults occur. However, the current mode and the continuous-valued states of a system are usually not directly observable and have to be estimated using the known actuation, available measurements and a model of the system. Hybrid systems theory provides a good way to model such systems by defining discrete modes of operation/failure and transition relations between them as well as a mode-dependent mathematical model. Nevertheless, estimating the state of such systems means facing an exponentially growing number of mode-sequences with their corresponding continuous evolution, which is computationally infeasible.

There exist several strategies to overcome this problem. Multiple model filtering approaches (Ackerson and Fu, 1970; Blom and Bar-Shalom, 1988; Li and Bar-Shalom, 1996; Semerdjiev and Mihaylova, 1998; Georges *et al.*, 2011), for example, reduce the number of filtering operations by mixing the estimation results for

all modes at every time-step. Particle filtering methods (de Freitas, 2002; Verma *et al*., 2004) estimate the probability distribution of the different mode/continuous state combinations. In the work of Narasimhan *et al*. (2004), a particle filtering approach is combined with a fault detection method to reduce the number of modes that need to be tracked by the particle filter. Hybrid estimation methods (Benazera *et al*., 2002; Hofbaur and Williams, 2002; Narasimhan and Biswas, 2002) derive likelihood measures to identify small sets of the most likely hypotheses and thus can deal with systems with a large number of modes. Benazera and Travé-Massuyès (2009) propose a set-membership hybrid estimation scheme which naturally merges hypotheses with identical mode estimates by calculating the convex hull of continuous estimates.

When used for diagnosis, all estimation approaches must find a way to deal with low probability-modes. Focusing on the most probable hypotheses is indeed conflicting with the fault modes being an order of magnitude less probable than normal modes. Koutsoukos *et al*. (2002) overcome this problem by using more particles, although this increases the computational cost. In the work of Dearden and Clancy (2002), the particle filter is based on importance sampling to ensure that fault modes obtain enough particles. On the other hand, hybrid diagnosis approaches (Bayoudh *et al*., 2008; Daigle *et al*., 2010) focus on the discrete part of the hybrid model and, using parity-space ideas (Gertler, 1991; Staroswiecki and Comet-Varga, 2001), limit the number of possible hypotheses to the number of modes in the system at each time step. However, additional state filtering operations need to be performed in order to obtain the continuous state estimate.

Most of the work cited above incorporate *a priori* defined mode transitions probabilities. However, defining probabilities *a priori* is a tedious and demanding task. Transitions to error modes can be determined based on failure probability analysis from operation feedback logs or by incorporating risk estimation. What is important to notice is that the result of this process considerably influences the behavior of the estimation algorithm. Thus, in this work we propose to define posterior transition probabilities by combining a hybrid estimation and a diagnosis approach. The benefit is two-fold; first, the chance of low probability modes to be considered is increased, when necessary, and second, we achieve a better focus on more relevant mode hypotheses, thus making the system less computationally intensive.

The paper is organized as follows. Section 2 formally introduces the hybrid model that we use. Section 3 reviews hybrid estimation in general. Section 4 describes the hybrid estimation approach and the parity-space method our algorithm relies on and introduces the combined algorithm. Section 5 describes a case study of a simulated satellite attitude control system while Section 6 shows the experimental results of the algorithm compared to existing hybrid estimation approaches.

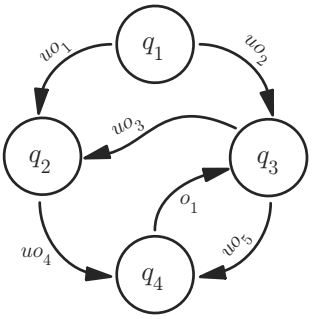

Fig. 1. Example of a discrete event system: automaton with four different states q_i and six possible mode transitions (observable events o_i and unobservable events uo_i).

2. Hybrid model

We use a hybrid model that is related to so-called linear-switched hybrid systems (Kamau and Lunze, 2003; Vidal *et al*., 2003) and combine a discrete event system with continuous dynamics in the sense of Henzinger (1996), as well as Hofbaur and Williams (2004).

Discrete event system. The discrete event system (see Fig. 1) is defined as an automaton with different states (modes of operation/failure) and transitions (discrete events) between them through the quadruple

$$M := (Q, \Sigma, T, Q_0), \tag{1}$$

where

- $Q = q_1, \ldots, q_l$ is the set of discrete states with $|Q| = l$. Each state $q_i \in Q$ represents a mode of operation or failure of the system.
- Σ is the set of events. Events correspond to steerable mode transitions, spontaneous mode changes and fault events. The subset $\Sigma_o \subseteq \Sigma$ denotes the set of observable events. Without loss of generality, we assume that fault events are unobservable.
- T is the (mode) transition function $T : Q \times \Sigma \rightarrow Q$ that captures the discrete evolution of the system.
- $Q_0 \in Q$ specifies the set of initial discrete states (modes).

Continuous-valued model. The underlying continuous-valued part of the model is defined through the (multi-mode) system

$$\Xi := (\zeta, Q, C, \zeta_0), \tag{2}$$

where

- ζ represents the set of continuous-valued variables that comprises n_u (exogenous) input variables

$$[u_{c,1}, \ldots, u_{c,n_u}]^T =: \mathbf{u}_c,$$

n_x state variables

$$[x_{c,1}, \ldots, x_{c,n_x}]^T =: \mathbf{x}_c,$$

and n_y output variables

$$[y_1, \ldots, y_{n_y}]^T =: \mathbf{y}_c$$

that represent the continuous-valued measurements.

- ζ_0 specifies the initial state of the continuous-valued state variables.

- C defines the set of system constraints that link the continuous variables and thus captures the continuous evolution of the automaton.

Within the scope of this paper, the system constraints C define a discrete-time linear model with sampling period T_s that associates each mode $q_i \in Q$ with a difference equation

$$\mathbf{x}_{c,k+1} = \mathbf{A}_i \mathbf{x}_{c,k} + \mathbf{B}_i \mathbf{u}_{c,k} + \mathbf{N}_i \mathbf{v}_{c,k} \tag{3}$$

and an algebraic equation that defines the measurements through

$$\mathbf{y}_{c,k} = \mathbf{C}_i \mathbf{x}_{c,k} + \mathbf{D}_i \mathbf{u}_{c,k} + \mathbf{M}_i \mathbf{v}_{c,k}, \tag{4}$$

where $\mathbf{x}_{c,k}$, $\mathbf{u}_{c,k}$ and $\mathbf{y}_{c,k}$ denote the valuation of the continuous state, input and output variables at time $t = kT_s$. The variable $\mathbf{v}_c := [v_{c,1}, \ldots, v_{c,n_x+n_y}]^T$ defines state noise $(v_{c,1}, \ldots, v_{c,n_x})$ and measurement noise $(v_{c,n_x+1}, \ldots, v_{c,n_x+n_y})$. The possibly mode-dependent magnitude of the disturbances is specified through the scaling vectors $\mathbf{n}_i$ and $\mathbf{m}_i$ that define the noise matrices $\mathbf{N}_i = [\mathrm{diag}(\mathbf{n}_i), \mathbf{0}]$, $\mathbf{M}_i = [\mathbf{0}, \mathrm{diag}(\mathbf{m}_i)]$ which select and scale the appropriate fraction of $\mathbf{v}_c$. In this paper, we assume that the system's dynamics within each mode are fully observable.

Hybrid model. The hybrid model is comprised of a discrete event system M accompanied by the multi-mode system Ξ:

$$S := (\zeta, Q, \Sigma, T, C, (Q_0, \zeta_0)). \tag{5}$$

Hybrid state. The hybrid state $\mathbf{x}_h$ of the system at time step k consists of the discrete state or mode $x_{d,k}$ and the associated continuous state $\mathbf{x}_{c,k}$:

$$\mathbf{x}_{h,k} = \langle x_{d,k}, \mathbf{x}_{c,k} \rangle . \tag{6}$$

3. Hybrid estimation

The task of *hybrid estimation* is to reconstruct both the mode of operation or failure of the system and the continuous-valued state variables at each time step. Indeed, the full continuous state and the current mode are usually not directly observable or measurable and the missing information has to be deduced from available measurements, known actuations and a model of the physical system. The main difficulty of this task is the close interaction of the discrete and the continuous behavior of the hybrid system. In theory, all possible mode transitions and the resulting mode sequences that can occur during the dynamic evolution of the system need to be taken into account. This results in an exponential growth in the number of mode sequence hypotheses.

Figure 2 shows the full hypotheses tree for three time steps for the system whose underlying DES is given in Fig. 1. The system starts from the (known) initial state q_3, i.e., at time step $k = 0$ we have a set $\mathbf{H_0} = \{H_0^{(1)}\}$ of $\lambda_0 = 1$ hypothesis[1]:

$$H_0^{(1)} = \langle\, \hat{\mathbf{x}}_{d,0}^{(1)} \,\rangle = \langle q_3 \rangle .$$

In the next time step, we derive all possible mode transitions from the discrete automaton M (see Eqn. (1)) and extend the existing hypothesis with the new mode estimates. In our specific case, we have to consider three possible (unobservable) mode transitions[2]: the self-transition $q_3 \rightarrow q_3$ and two unobservable transitions to modes q_2 and q_4, respectively. We repeat this process recursively as time elapses. The result encodes an exponentially growing hypotheses tree (see Fig. 2 for the tree at $k = 2$ with $\lambda_2 = 6$ hypotheses). Each path in the tree represents a mode-sequence hypothesis that defines a distinct time-varying continuous model for the system's evolution.

It is easy to see that even with a moderate number of possible modes this task becomes computationally infeasible after a few time steps. To overcome this problem, suboptimal methods were developed that merge or prune mode sequence hypotheses and/or deduce appropriate likelihood measures to focus on a possibly small set of most likely hypotheses. On the other hand, hybrid diagnosis schemes were proposed that focus on the mode estimate only. Thus, hybrid diagnosis neglects the *value* of the continuous *state variables*. Hybrid diagnosis employs, for example, mode consistency tests that validate mode hypotheses against input/output relations (for sequences of continuous inputs $\mathbf{u}_{c,k}$ and continuous outputs $\mathbf{y}_{c,k}$). As a consequence, at most l mode

[1] The superscript (i) of the individual $H_j^{(i)}$ is used to enumerate mode sequence hypotheses, whereas the subscript j indicates the associated time step.

[2] We process the non-transition $q_j \rightarrow q_j$ as an additional transition.

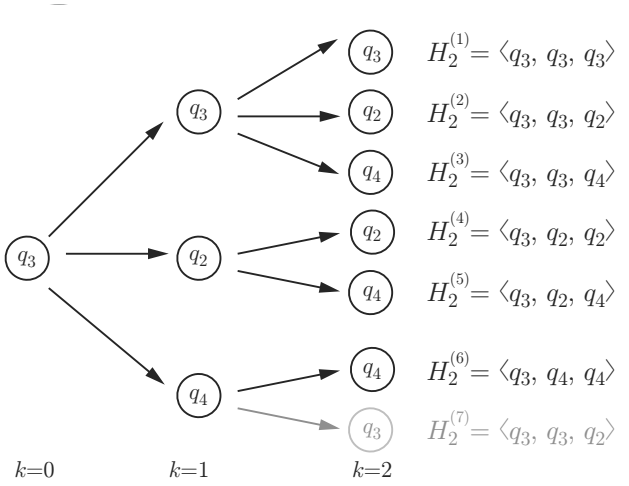

Fig. 2. Hypotheses tree. Every node represents a mode hypothesis. A path from the root node to the leaves defines a mode sequence hypothesis. The last hypothesis, $H_2^{(7)}$, is greyed out, since the mode transition from q_4 to q_3 is observable and could not be observed in this specific case.

hypotheses need to be checked per time step, where l denotes the number of modes in the system and thus avoids the exponential explosion that comes with mode-sequence hypotheses.

4. Synergetic hybrid estimation

We propose to build upon both schemes, hybrid estimation and hybrid diagnosis, to obtain a synergetic scheme for hybrid estimation that utilizes the advantages of both the approaches. The hybrid state estimation algorithm that we use, hME (Hofbaur and Williams, 2004; Hofbaur, 2005), labels every mode sequence hypothesis under consideration with a probability-like belief. This approach enables the algorithm to focus on the set of the most likely hypotheses.

The second component is a hybrid diagnosis scheme that employs a parity-space consistency check (Gertler, 1991). This algorithm is used to achieve a better focus (of hME) on hypotheses consistent with that test and thus helps to avoid unnecessary filtering operations. Both algorithms and their interaction will be described in the following sections.

4.1. Hybrid mode estimation algorithm. The hybrid Mode Estimation (hME) algorithm was originally developed for probabilistic hybrid automata and their concurrent composition. These probabilistic models utilize Hidden Markov Models (HMMs) as the automaton model. This original framework provides *prior transition probabilities* that help hME to focus on likely estimation hypotheses. Specifying proper values for the prior

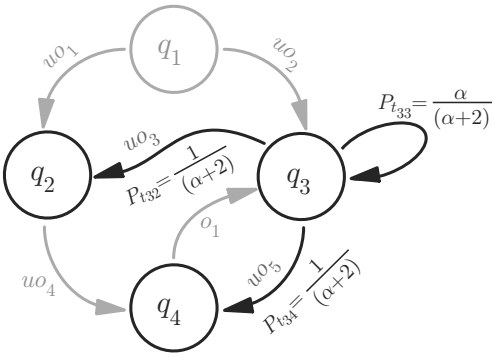

Fig. 3. Mode transition probability specification for mode q_3 with $n = 2$ unobservable transitions.

probabilities of the mode transitions in hybrid models is a challenge. The DES automaton model (Eqn. (1)) utilizes a simpler transition definition without explicit prior probability specification for mode transitions. Nevertheless, we want to utilize the modelling assumption that mode transitions occur infrequently, thus a priori it is more likely that the mode remains unchanged.

This assumption is reasonable, since the occurrence of a fault usually has a low probability. Furthermore, transitions between nominal operating modes occur infrequently in relation to the sampling time. We express this fact through an automated specification for transition likelihood as follows: The estimator assumes that it is α times ($\alpha > 1$) more likely that the mode of operation remains unchanged. As a consequence, we specify the *a priori* transition probabilities

$$P(t_{ij}) = \begin{cases} P_{t_{ii}} = \dfrac{\alpha}{(\alpha+n)} & \text{for the non-transition } q_i \rightarrow q_i \\ P_{t_{ij}} = \dfrac{1}{(\alpha+n)} & \text{for outgoing transitions } q_i \rightarrow q_j, i \neq j \end{cases} \tag{7}$$

where n denotes the number of outgoing transitions from a specific mode that cannot be observed directly and α defines the probability ratio that a user of hME can select.

Figure 3 depicts an example for mode q_3 with $n = 2$ outgoing transitions. The choice of α can, for example, be based on known error rates of the involved components. In case the system contains observable transitions (events), we define *conditional* probabilities for any observable mode transition t_{ij}:

$$\begin{aligned} P(t_{ij}|o_{ij}) &= 1, \\ P(t_{ij}|\overline{o_{ij}}) &= 0\,. \end{aligned} \tag{8}$$

The remaining transitions are labeled with the above specified prior probabilities (Eqn. (7)) in case the event could not be observed. However, if the event can be observed, the other transitions from that mode obtain the

conditional probability

$$P(t_{ik}|o_{ij}) = 0, \quad k \neq j \; . \tag{9}$$

With this mode transition classification we can specify the hME estimation procedure as a two-step search procedure that is guided by a belief update process as follows: At the beginning, every initial state hypothesis is assigned a belief b_0. The first step (transition expansion) calculates the possible immediate (mode) successors and the prior probability distribution $\bar{b}_{k|k-1}$ based on the above specified transition probabilities. The second step (continuous estimation) deduces the corresponding continuous state estimates as well as the final belief b_k of the hypotheses. To illustrate this update procedure, we reconsider the hybrid model from Fig. 1. Again, we assume a known initial state of the system and start with the singleton $\mathbf{H}_0 = \{H_0^{(1)}\}$:

$$H_0^{(1)} = \langle\, \hat{\mathbf{x}}_{d,0}^{(1)} \,\rangle = \langle q_3 \rangle \,,$$
$$b(H_0^{(1)}) = 1.$$

Expanding the hypotheses tree with all three mode transition possibilities leads to the new set $\overline{\mathbf{H}}_1$ with $\lambda_1 = 3$ mode sequence hypotheses. The prior belief $\bar{b}_{k|k-1}$of these new hypotheses is obtained by multiplying the belief of the parent node (in our case this is the root node with $b_0^{(1)} = 1$) with the appropriate transition probabilities specified according to Eqn. (7). In the second step we compute the value of the appropriate continuous state estimates $\hat{\mathbf{x}}_{c,1}^{(i)}$, $i = 1, 2, 3$, for the new mode sequence hypotheses. This requires individual Kalman filters as each hypothesis specifies a unique combination of the mode $\hat{\mathbf{x}}_{d,k}$ and the continuous estimate $\hat{\mathbf{x}}_{c,k}$. The belief values of the hypotheses are updated using the observation function $P_{\mathcal{O}}^{(i)} = p(\mathbf{y}_{c,k}|\hat{\mathbf{x}}_{c,k|k-1}^{(i)}, \mathbf{u}_{c,k})$ obtained in the second step of the Kalman filtering process; more precisely, we omit the normalization term and utilize a modified observation function $\overline{P}_{\mathcal{O}}^{(i)}$ that is defined by the multi-variate Gaussian distribution

$$\overline{P}_{\mathcal{O}}^{(i)} = \exp(-0.5\mathbf{r}_{i,k}^T \mathbf{S}_{i,k}^{-1} \mathbf{r}_{i,k}),$$

where $\mathbf{r}_{i,k}$ along with the corresponding covariance matrix $\mathbf{S}_{i,k}$ define the innovation of the i-th hypothesis:

$$\mathbf{r}_{i,k} = \mathbf{y}_{c,k} - \mathbf{C}_i \hat{\mathbf{x}}_{c,k|k-1}^{(i)} - \mathbf{D}_i \mathbf{u}_{c\,,k} \quad i = 1, 2, 3.$$

The final belief of the three hypotheses in $\overline{\mathbf{H}}_1$ can now be computed by multiplying the prior belief $\bar{b}_{k|k-1}(H_1^{(i)})$, $i = 1, 2, 3$, from the previous step with the value of the appropriate observation function $\overline{P}_{\mathcal{O}}^{(i)}$. This results in the new set $\mathbf{H}_1$ that contains the three possible mode sequences along with their updated probabilities.

Figure 4 visualizes the two-step hybrid estimation process for this example.

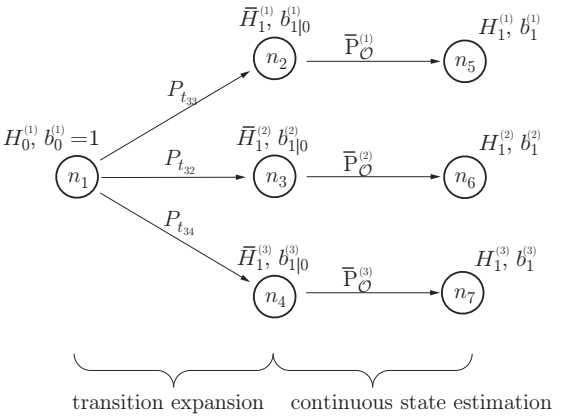

Fig. 4. Example of the two-step update procedure for the probability distribution of the hypotheses.

In order to efficiently compute the set of the most likely hypotheses only, we frame the hypothesis tree expansion procedure as a search procedure with path costs based on the logarithm of the belief values defined above. This path cost is used to guide a best-first search procedure that determines the most likely hypotheses in descending order. We use *A*search*, a variant of best-first search that employs the evaluation function

$$f(n_i) = g(n_i) + h(n_i) \tag{10}$$

which is comprised of the cost so far $g(n_i) = -\log(b_{k-1})$ and an estimated cost to go $h(n_i)$ for a node n_i in the hypotheses tree. A* needs an admissible heuristic in order to provide the optimal result, i.e., the cost to go must not be overestimated. The search algorithm of hME uses the transition probabilities as defined in (7)–(9) to estimate the cost to go. This ensures that the cost is never overestimated as the observation probability always satisfies

$$P_{\mathcal{O}}^{(i)} \leq 1$$

and thus

$$h(n_i) = -\log(P_{\mathcal{T}}) \leq -\log(P_{\mathcal{T}}) - \log(P_{\mathcal{O}}).$$

However, in the case of a mode transition, this procedure might highly underestimate the actual cost which downgrades the performance of the algorithm and, in some cases, mode-change detection is delayed for several time steps until the influence of the filtering operation is high enough.

This is where the above mentioned hybrid diagnosis approach (Bayoudh *et al.*, 2008) comes into play. It defines input/output relations for the different modes of operation. The evaluation of these relations allows for the definition of posterior transition probabilities.

4.2. Hybrid diagnosis through parity-space methods. Following the ideas of Bayoudh *et al*. (2008), we derive for the modes $q_i \in Q$ of the hybrid system S (Eqn. (5)) a set of Analytical Redundancy Relations (ARRs) that relate the continuous inputs to the observable continuous outputs over a time-window of length $p+1$. Selecting p appropriately (typically, $p \leq n_x$) allows us to eliminate any dependencies on the system's continuous state $\mathbf{x}_c$. This standard procedure from FDI (Gertler, 1991) can be summarized for a particular mode q_i of our hybrid system as follows: We stack the input, output and noise of the last $p+1$ time steps according to

$$\begin{aligned} \mathbf{U}_k &:= [\mathbf{u}_{c,k-p}^T, \ldots, \mathbf{u}_{c,k}^T]^T, \\ \mathbf{Y}_k &:= [\mathbf{y}_{c,k-p}^T, \ldots, \mathbf{y}_{c,k}^T]^T, \\ \mathbf{V}_k &:= [\mathbf{v}_{c,k-p}^T, \ldots, \mathbf{v}_{c,k}^T]^T \end{aligned} \tag{11}$$

and obtain for the continuous evolution equations (3) and (4) in mode q_i

$$\begin{aligned} \mathbf{Y}_k = \mathbf{O}_i \mathbf{x}_{c,k-p} &+ \mathbf{L}_i(\mathbf{A}_i, \mathbf{B}_i, \mathbf{C}_i, \mathbf{D}_i)\mathbf{U}_k \\ &+ \mathbf{L}_i(\mathbf{A}_i, \mathbf{N}_i, \mathbf{C}_i, \mathbf{M}_i)\mathbf{V}_k, \end{aligned} \tag{12}$$

with the matrices

$$\mathbf{O}_i := \begin{bmatrix} \mathbf{C}_i \\ \mathbf{C}_i\mathbf{A}_i \\ \vdots \\ \mathbf{C}_i\mathbf{A}_i^p \end{bmatrix} \tag{13}$$

and

$$\begin{aligned} &\mathbf{L}_i(\mathbf{A}_i, \mathbf{B}_i, \mathbf{C}_i, \mathbf{D}_i) \\ &:= \begin{bmatrix} \mathbf{D}_i & \mathbf{0} & \cdots & \mathbf{0} \\ \mathbf{C}_i\mathbf{B}_i & \mathbf{D}_i & \ddots & \vdots \\ \vdots & \ddots & \ddots & \mathbf{0} \\ \mathbf{C}_i\mathbf{A}_i^{p-1}\mathbf{B}_i & \cdots & \mathbf{C}_i\mathbf{B}_i & \mathbf{D}_i \end{bmatrix}. \end{aligned} \tag{14}$$

In order to obtain a parity relation, we need to eliminate the continuous state $\mathbf{x}_{c,k-p}$ from Eqn. (12). Increasing the length of the time-window adds additional rows to the matrix $\mathbf{O}_i$ whereas the number of columns remains at n_x (the number of continuous states of the model). Thus, for a sufficiently large p, we can always find a matrix $\mathbf{\Omega}_i$ that fulfills $\mathbf{\Omega}_i\mathbf{O}_i = \mathbf{0}$[3]. Hence, we can define the residual vector

$$\begin{aligned} \mathbf{r}_{i,k} := \mathbf{\Omega}_i\mathbf{Y}_k &- \mathbf{\Omega}_i\mathbf{L}_i(\mathbf{A}_i, \mathbf{B}_i, \mathbf{C}_i, \mathbf{D}_i)\mathbf{U}_k \\ &- \mathbf{\Omega}_i\mathbf{L}_i(\mathbf{A}_i, \mathbf{N}_i, \mathbf{C}_i, \mathbf{M}_i)\mathbf{V}_k\,. \end{aligned} \tag{15}$$

For the sake of simplicity, we will explain the algorithm for the noise-free case where we can omit the term $\mathbf{\Omega}_i\mathbf{L}(\mathbf{A}_i, \mathbf{N}_i, \mathbf{C}_i, \mathbf{M}_i)\mathbf{V}_k$ and have to check the ARR consistency simply through

$$\mathbf{r}_{i,k} = [r_{i1,k}, \ldots, r_{im_i,k}]^T = \mathbf{0}. \tag{16}$$

The influence of noise on the algorithm is explained in greater detail in Section 4.4.

[3]For further conditions on the existence of such a matrix $\mathbf{\Omega}_i$ refer to the work of Chow and Willsky (1984).

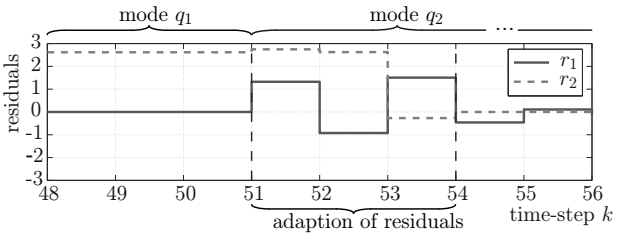

Fig. 5. Residuals of mode q_1 and q_2.

Settling time of the residuals. The residual equations for hybrid systems are derived assuming a constant mode over the length of the observation window $p+1$, i.e., the equations are only valid if the system operates at a constant mode. A mode change results in an abrupt change of the residuals' values. After the transition, the residuals of the new mode need at least p time steps to settle and provide a mode information again.[4] During this transition phase, a purely residual based mode estimator is not able to provide a mode information. This behavior is illustrated in Fig. 5 with a mode change from mode q_1 to q_2 at time step $k = 51$ and an observation window of length $p+1 = 4$. The residual r_1 of mode q_1 changes its value immediately after the transition. The residual r_2 of mode q_2 needs $p = 3$ additional time steps to settle.

Non-discernible modes and delayed mode change detection. In some cases the evaluation of the residual equations does not result in a uniquely identifiable mode but provides several hypotheses that are consistent with the ARRs. A mode transition between two such modes, however, can usually still be observed. Furthermore, all other modes can be excluded and the set of hypotheses limited. Two modes that show identical input/output behaviour and thus provide the same residual information are called non-discernible modes in the literature (Cocquempot *et al*., 2004; Bayoudh *et al*., 2008). This property can be determined by the following test: Two modes are called non-discernible if for an observation window with $p = n_x$

$$\text{rank}(\mathbf{O}_i) = \text{rank}(\mathbf{O}_j) = \text{rank}([\mathbf{O}_i, \mathbf{O}_j, \mathbf{\Delta}_{ij}]) \tag{17}$$

with $\mathbf{\Delta}_{ij} = \mathbf{L}_i - \mathbf{L}_j$ ($\mathbf{L}$ is defined in Eqn. (14)).

[4]In the presence of noise, mode estimation requires additional time (τ_{filter}), since we need to filter the residuals in order to avoid wrong mode predictions.

Furthermore, the detection of a mode change (i.e., the change of the residuals' values) of two discriminable modes can be *delayed* for one or several time steps.

In summary, mode estimation through parity space methods provides good mode estimates. For larger numbers of modes, however, many parity relations need to be evaluated. In order to obtain the continuous state estimate, one has to perform additional state filtering operations. In the vicinity of mode transitions, the mode estimate from the parity space estimator cannot be used directly for the choice of the adequate continuous-valued model due to the above-mentioned settling time (Rienmüller *et al.*, 2009). In addition, the diagnoser-based mode estimator would fail to track several mode changes within the observation window. For non-discernible modes, additional information is necessary in order to determine the correct mode and thus perform the continuous filtering operations. Furthermore, in the presence of noise, decoupling procedures that are not in the scope of this paper are required.

The hybrid mode estimation algorithm, on the other hand, provides an estimate for both the continuous and the discrete state of the system. The adaption phase of the continuous state estimate after a mode transition can be reduced significantly, since the algorithm is able to track several possible state hypotheses concurrently. However, a better focus on highly probable hypotheses would reduce the computational cost of the algorithm. Furthermore, the definition of mode transition probabilities is not obvious. hME and other probability based methods face the problem that mode transitions to failure modes with *a priori* probabilities, e.g., defined based on error rates of the system and the components used, and thus classified unlikely, are hardly considered by the algorithms. This has the effect that the algorithms have to define "artificial" probability distributions that are often hard to legitimate. Combining the hybrid mode estimation algorithm with the residual based diagnosis approach allows us to cope with this problem.

4.3. Synergetic hybrid mode estimation. The original search procedure of hME deduces the most promising hypotheses based on the cost so far and *a priori* defined transition probabilities only (see Eqn. (7)). The new synergetic hybrid estimation scheme proposed in this section allows for the definition of *posterior* transition probabilities between the modes of the hybrid automaton. Evaluating the analytic redundancy relations, we obtain additional information about the likelihood of hypotheses assuming a constant mode over the last $p+1$ time steps. If the evaluation of the residual vector $\mathbf{r}_i$ (Eqn. (16)) of mode q_i results in a contradiction, new transition probabilities are defined for the specific modes

$$P(t_{ii}|\mathbf{r}_i \neq \mathbf{0}) = 0 \quad \text{for } q_i \rightarrow q_i,$$

$$P(t_{ij}|\mathbf{r}_i \neq \mathbf{0}) = P_{t_{ij}} \cdot \frac{1}{c} \quad \text{for } q_i \rightarrow q_j,\ i \neq j, \tag{18}$$

with

$$c = \sum_{j,j\neq i} P_{t_{ij}}.$$

In our specific setting for $P_{t_{ij}}$ (Eqn. (7)) we simply obtain

$$P(t_{ij}|\mathbf{r}_i \neq \mathbf{0}) = \frac{1}{n} \quad \text{for } q_i \rightarrow q_j,\ i \neq j.$$

These refined transition probabilities allow us to eliminate inappropriate mode sequence hypotheses prior to the computationally intensive continuous filtering step of the hME algorithm.

In case the residuals evaluate to zero, we leave the transition probabilities unchanged, since the detection of a mode change by means of mode specific analytical redundancy relations has some limitations (cf. Section 4.2): the change of the residuals' value can indeed be delayed for one or several time steps or several different modes can be non-discernible and thus cannot provide a unique result. Additionally, in the presence of noise and/or parameter uncertainties, the residuals are not zero exactly (cf. Section 4.4). Applying a conservative threshold reduces the number of false alarms. However, this could lead to residuals wrongly lying in between the specified bounds.

To make the process of posterior probability specification clear, we reconsider the example from Section 2 (Fig. 1). During hybrid mode estimation, a hypothesis $\{H_k^{(j)}\}$ is generated that assumes a constant mode q_3 over the last p time steps, i.e., $x_{d,k-p} = \cdots = x_{d,k-1} = q_3$. Now we can evaluate the transition $q_3 \rightarrow q_3$ by computing the residuals for mode q_3 at time step k. Recall that the parity-equations are defined for a system with a constant mode over $p+1$ time steps. Thus, we can evaluate the mode-sequence $x_{d,k-p} = \cdots = x_{d,k-1} = x_{d,k} = q_3$ by means of Eqn. (15). Specifically, there are two possible results: first, the assumption of mode q_3 does not contradict the result of the residuals, i.e., $\mathbf{r}_{3,k} = \mathbf{0}$, second, the evaluation of the residuals implies that the assumption that the system still remains in mode q_3 is not correct. In this latter case, we can update the transition probabilities from mode q_3 (see Eqn. (7), with $\alpha = 3$) as follows[5]:

$$P(q_3 \rightarrow q_3|\mathbf{r}_{3,k} \neq \mathbf{0}) = 0,$$
$$P(q_3 \rightarrow q_2|\mathbf{r}_{3,k} \neq \mathbf{0}) = 0.2 \cdot \frac{1}{c} = 0.5,$$
$$P(q_3 \rightarrow q_4|\mathbf{r}_{3,k} \neq \mathbf{0}) = 0.2 \cdot \frac{1}{c} = 0.5\,.$$

[5] If mode q_3 was not approved by the residuals at time step $k-1$, the probability update can only be made for hypotheses assuming a constant mode q_3 up to time step $k-1$ and not for the transition $q_3 \rightarrow q_3$ in general.

Hence, the formerly unlikely transitions to modes q_2 and q_4 are now classified more likely and hME will tend to select them. However, if all residual equations of mode q_3 evaluate to zero, we leave the transition probabilities unchanged (the self-transition is already assigned a higher probability),

$$P(q_3 \rightarrow q_3 | \mathbf{r}_{3,k} = \mathbf{0}) = P_{t_{ii}} = 0.6.$$

The combination of hME with the ARR based diagnosis method results in an improved search procedure. The benefit is twofold: first, we can eliminate all hypotheses that are not consistent with the ARRs *before* the costly filtering operation and thus save computing time second, the altered transition probabilities increase the chance of a mode transition, formerly classified unlikely, to be considered by the algorithm.

Consequences of non-discernible modes. In Section 4.2 the particularity of non-discernible modes was introduced. As a result of this property, the residuals show the same behaviour for several non-discernible modes. Evaluating the residuals for these modes does not provide enough evidence to diagnose the specific mode. However, when a mode and its successor are non-discernible, the mode transition can still be observed (in almost all cases) through a change in the residual. The evaluation to non-zero is due to the mode transition within the observation window used to evaluate the residuals, i.e., to discontinuities, possibly of high order, in the signals involved in the computational form of the residuals at transition time (Hofbaur *et al*., 2010).

4.4. Noise impact on the synergetic hybrid mode estimation algorithm. In order to account for noise in the residual vector, we define a noise matrix (cf. Eqn. (15))

$$\mathbf{W}_i := \text{abs}(\mathbf{\Omega}_i)\mathbf{L}(\mathbf{A}_i, \mathbf{N}_i, \mathbf{C}_i, \mathbf{M}_i)$$

for every mode q_i that captures the influence of the disturbances within the observation window of length $p+1$. If we model the disturbances through random variables v with $|v| \leq 1$, we can compute bounds ε_{ij} for the j-th residual $r_{ij,k}$ for mode i at time step k by taking the sum over the j-th line of $\mathbf{W}_i$, i.e.,

$$\varepsilon_{ij} := \sum_{k=1}^{p(n_x+n_y)} w_{jk}, \quad j = 1, \ldots, m\,. \tag{19}$$

With this information, we can rewrite the consistency check

$$\tilde{r}_{ij,k} := \begin{cases} 0 \text{ if } |r_{ij,k}| \leq \varepsilon_{ij}, \\ 1 \text{ otherwise} \end{cases} \tag{20}$$

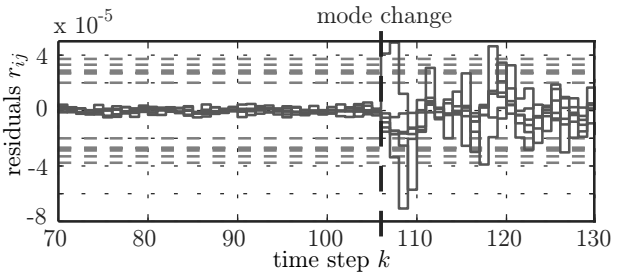

Fig. 6. Residuals for mode q_i (solid lines) with appropriate bounds (dashed lines) to account for process and measurement noise. At time $k = 106$ a mode transition takes place. As a result, the residual values surpass the specified bounds.

$j = 1, \ldots, m_i$, and obtain a Boolean residual vector for mode q_i at time step k as

$$\tilde{\mathbf{r}}_{i,k} := [\tilde{r}_{i1,k}, \ldots, \tilde{r}_{im_i,k}]^T. \tag{21}$$

Figure 6 depicts a sample run of residuals before and after a mode transition (at time step $k = 106$). The dashed lines mark the individual bounds ε_{ij}. Before the mode transition, the residuals remain within the bounds. Afterwards, the residual values surpass the bounds.

5. Case study: The attitude control system

Satellites are typical examples for autonomously operating robotic systems. The Attitude Control System (ACS) for the three-axes stabilization of a satellite is critical for its autonomous operation (Olive, 2012). We therefore use a (simplified) model of an ACS that includes several nominal modes and faults to test the health monitoring and diagnosis capabilities of our hybrid estimation scheme.

5.1. System's modes of operation or failure. The system is assumed to have two nominal modes, q_1 and q_2. A switch from one nominal mode to the other can only be achieved by a command. In mode q_2 the instantaneous rotation vector of the target attitude frame C relative to the inertial frame R expressed in the target attitude frame C becomes $\mathbf{\Omega}^{[C]}_{C/R} = \begin{bmatrix} 0 & \omega_0 & 0 \end{bmatrix}^T$. All other modes are fault modes that model the behaviour of the system in the case of one or several wheels going into saturation.

State space equations. A detailed description of the modeling process can be found in Appendix. We suppose that we command the wheel acceleration and we do not consider the saturation problem, hence the input vector is defined as

$$\mathbf{u}_c = \begin{bmatrix} u_1 \\ u_2 \\ u_3 \end{bmatrix} = \begin{bmatrix} \ddot{\theta}_X \\ \ddot{\theta}_Y \\ \ddot{\theta}_Z \end{bmatrix}.$$

The output vector is defined by the sensor output

$$\mathbf{y}_c = \begin{bmatrix} p \\ q \\ r \end{bmatrix}.$$

The vector of the continuously valued state variables consists of the Cardan angles (see Fig. A2) and their first derivative with respect to time:

$$\mathbf{X} = \begin{bmatrix} \theta_R & \theta_T & \theta_L & \dot{\theta}_R & \dot{\theta}_T & \dot{\theta}_L \end{bmatrix}^T.$$

Using these definitions, we obtain the state space representation of the satellite attitude control system

$$\begin{aligned} \dot{\mathbf{x}}_c &= \mathbf{A}_i \mathbf{x}_c + \mathbf{B}_i \mathbf{u}_c, \\ \mathbf{y}_c &= \mathbf{C}_i \mathbf{x}_c + \mathbf{W}_i, \end{aligned} \tag{22}$$

$i = 1, \ldots, l$, with

$$\mathbf{A}_1 = \begin{bmatrix} 0 & 0 & 0 & 1 & & \\ 0 & 0 & 0 & 0 & & \\ 0 & 0 & 0 & 0 & & \\ 0 & 0 & 0 & 0 & & \\ 0 & 0 & 0 & 0 & & \\ 0 & 0 & 0 & \left(\frac{I_Y - I_X}{I_Z} - 1\right)\omega_0 & & \\ & & & & 0 & 0 \\ & & & & 1 & 0 \\ & & & & 0 & 1 \\ & & & & 0 & \left(\frac{I_Z - I_Y}{I_X} + 1\right)\omega_0 \\ & & & & 0 & 0 \\ & & & & 0 & 0 \end{bmatrix},$$

$$\mathbf{B}_1 = \begin{bmatrix} 0 & 0 & 0 \\ 0 & 0 & 0 \\ 0 & 0 & 0 \\ -\frac{I_W}{I_X} & 0 & 0 \\ 0 & -\frac{I_W}{I_Y} & 0 \\ 0 & 0 & -\frac{I_W}{I_Z} \end{bmatrix},$$

$$\mathbf{C}_1 = \begin{bmatrix} 0 & 0 & -\omega_0 & 1 & 0 & 0 \\ 0 & 0 & 0 & 0 & 1 & 0 \\ \omega_0 & 0 & 0 & 0 & 0 & 1 \end{bmatrix},$$

$$\mathbf{W}_1 = \begin{bmatrix} 0 \\ -\omega_0 \\ 0 \end{bmatrix}$$

for the nominal mode q_1. The fault modes represent the case that one or several wheels go into saturation. As an example, mode q_4 with wheel 2 in saturation is shown:

$$\mathbf{A}_4 = \mathbf{A}_1, \quad \mathbf{B}_4 = \begin{bmatrix} 0 & 0 & 0 \\ 0 & 0 & 0 \\ 0 & 0 & 0 \\ -\frac{I_W}{I_X} & 0 & 0 \\ 0 & 0 & 0 \\ 0 & 0 & -\frac{I_W}{I_Z} \end{bmatrix},$$

$$\mathbf{C}_4 = \mathbf{C}_1, \ \mathbf{W}_4 = \mathbf{W}_1.$$

Approximation values used for the simulation are

$$\begin{aligned} I_X &= 600 \text{ kg m}^2, \\ I_Y &= 700 \text{ kg m}^2, \\ I_Z &= 600 \text{ kg m}^2, \\ I_W &= 0.1322 \text{ kg m}^2, \\ \omega_0 &= 2.10^{-2} \text{ rad/s}. \end{aligned}$$

6. Experimental results

In our experiments we compared the mode and continuous state estimation abilities of our synergetic hybrid mode estimation algorithm with existing hybrid estimation and diagnosis schemes, such as the Interacting Multiple Model (IMM) algorithm (see, e.g., Blom and Bar-Shalom, 1988), the hME algorithm (Hofbaur and Williams, 2002) and a parity space Hybrid Diagnosis (HyDiag) approach (Bayoudh *et al.*, 2008).

6.1. Experimental setup. The experiments are based on the model for the satellite attitude control system (see Section 5). A detailed derivation of the different nominal and fault modes can be found in Appendix. Figure 7 depicts part of the discrete automaton of the hybrid model. For the sake of simplicity, we omit mode q_2 and the corresponding fault modes q_i, $i \in \{6, 7, 8, 13, 14, 15, 16\}$. Modes q_3, q_4 and q_5 represent fault modes with reaction wheel 1, 2 or 3 going into saturation, respectively. Modes $q_{9,10,11}$ represent double faults with two wheels in saturation and mode q_{12} the case in which all wheels are in a fault mode. For the experimental setup, we define the appropriate set $\tilde{Q} = \{q_1, q_3, q_4, q_5, q_9, q_{10}, q_{11}, q_{12}\}$.

For the experiments presented in this paper, we assume bounded noise with $\mathbf{v}_{c\,i,x} \leq 5 \cdot 10^{-6}$ and $\mathbf{v}_{y\,i,x} \leq$

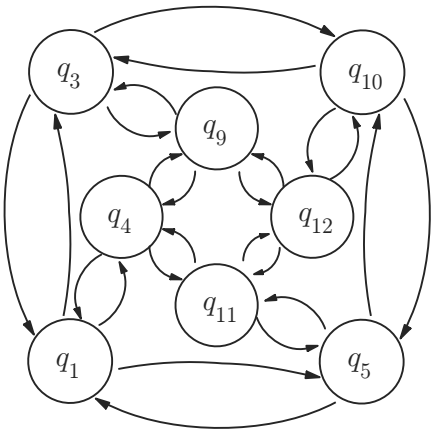

Fig. 7. Discrete event system of the hybrid model.

$6 \cdot 10^{-6}$ for all modes q_i of the system. The tests were performed with randomized continuous input sequences leading to different sequences of failure modes.

The obtained mode sequences of the test runs are estimated using several hybrid estimation methods. First, we use an optimal algorithm that is aware of the actual mode sequence. This gives us an optimal bound on the relative error for the continuous estimation. Then, we compare the estimation results of our new synergetic Hybrid Mode Estimation (synHME) scheme to the results of an interacting multiple model estimator, a parity space hybrid diagnoser and the hybrid mode estimation algorithm. Figure 8 depicts the mode sequence of a sample test run with mode transitions specified through $\alpha = 3$ (see Eqn. (7)), with one wheel going into saturation at time step $k = 192$.

For the sake of clarity, Fig. 8 depicts wrong mode classifications only for the IMM as well as the HyDiag method and hME. For all other time steps, the mode was correctly identified. The hybrid mode estimator (dashed line) fails to track the transition from the nominal mode q_1 to the failure mode q_3. Since the input/output dynamics of both modes are similar to each other, the prior transition probabilities distort the estimation result. Due to the higher *a priori* self transition probability, mode q_1 is still considered the most probable. With synHME, the mode transition from the nominal mode q_1 to failure mode q_3 can be recognized (solid line) and the algorithm is able to follow the system's mode exactly. The IMM estimator (diamonds) identifies the switch between the nominal and the failure mode. However, especially when the system is in the nominal mode, several mode estimation errors occur. The HyDiag method recognizes the mode transition at $k = 192$, but the identification of the new mode takes additional time steps due to the required settling time of the residuals. Table 1 depicts the average estimation results of 15 test runs with 130 time steps each for all algorithms.

The results are compared regarding continuous and discrete state estimation quality and the number of filtering operations. The IMM uses $|\tilde{Q}| = l = 8$ filters per time step. hME and synHME compute the leading set of λ hypotheses. In our case we use a fringe size of $\lambda = 3$ for hME and $\lambda = 2$ for synHME. However, the algorithms require in general $f \geq \lambda$ filter operations per time step in order to derive this leading set. In average, however, we observed that f is only slightly larger than λ. The IMM and the new synHME show similar abilities concerning the hybrid estimation quality. However, the number of filtering operations can be reduced. hME has a worse performance regarding the mode estimation capabilities. This is due to the fact that the continuous dynamics are quite similar and thus the influence of the prior mode transition probabilities is considerable. synHME, however, overcomes this problem and identifies the correct mode at a rate of 97.95%.

Table 1. Comparison of the hybrid estimation results obtained by an IMM estimator, the purely hybrid diagnosis based estimator (HyDiag), hME and the new synergetic hME.

algorithm	**rel. error xc** e	**correct mode** [%]	**filter calls** (average)
optimal	0.086	100	1
synhME	0.086	97.95	4.2
hME	0.0864	87.9	5.05
IMM	0.062	96.6	8
HyDiag	0.0865	91.5	1

7. Conclusion

This paper presents a novel hybrid estimation/diagnosis scheme to overcome conceptual difficulties with traditional hybrid estimation and improve the run-time behavior of this demanding task. It builds upon a hybrid estimation algorithm and a diagnosis scheme for hybrid systems to combine their complementary advantages. The hybrid mode estimation algorithm can deal well with a large number of modes, since it focuses on a small set of the most likely mode hypotheses. Focusing builds upon prior information for the mode transitions, i.e., the prior mode transition probabilities, and information drawn from a consecutive continuous filtering step.

Defining the prior transition probabilities for the system's model is, however, a tedious process and has strong impact on estimation quality and the runtime performance of the algorithm. Our approach was to simplify the prior-probability specification and to supplement the estimation process with additional posterior transition probability information. This information is drawn from the hybrid diagnosis scheme HyDiag that applies a parity space approach for transition detection and mode estimation.

This synergetic combination of two estimation/diagnosis schemes implies redundant operations. However, the complementary strengths of both schemes, continuous filtering and mode identification of hME and mode transition detection of HyDiag's parity space approach, respectively, significantly improve the focusing capabilities of the combined algorithm. This improved focus on the most likely hypotheses compensates the redundant/complementary filtering operations and thus improves the quality of the hybrid estimation result whilst keeping the computationally efficiency of hME.

References

Ackerson, G. and Fu, K. (1970). On state estimation in switching environments, *IEEE Transactions on Automatic Control*

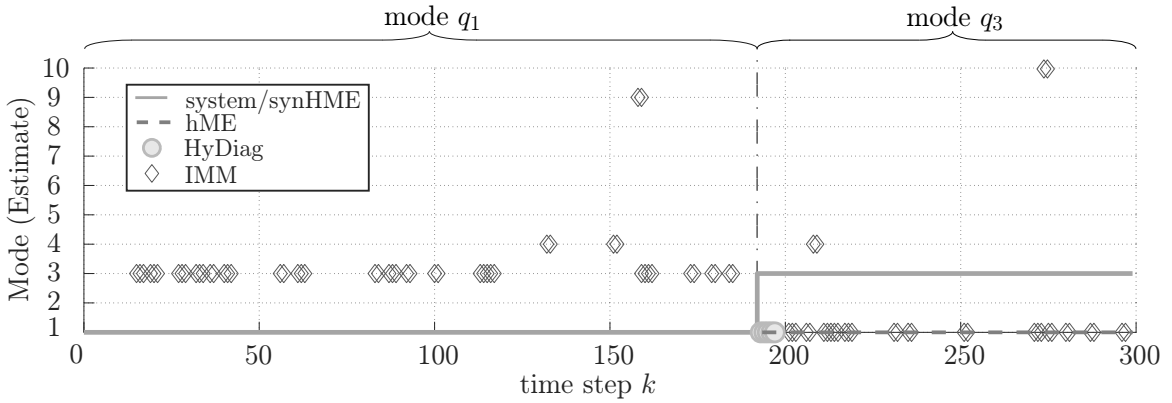

Fig. 8. Mode estimation (errors). The picture shows an excerpt of the experiments. In this example, the system starts in the nominal mode q_1. At time step $k = 192$, wheel 1 goes into saturation (mode q_3 of the system). Here synHME is able to follow the system's mode exactly (solid line). hME fails to track the mode transition and the IMM gives several false alarms while the system is in the nominal mode and assumes the nominal mode q_1 while wheel 1 is saturated (mode q_3). The HyDiag method identifies the correct mode q_3 with a delay due to the required settling time of the residuals. The figure shows wrong mode estimates only for the IMM as well as HyDiag and hME. For all other time steps, the algorithms identified the correct mode.

15(1): 10–17.

Bayoudh, M., Travé-Massuyès, L. and Olive, X. (2008). Hybrid systems diagnosis by coupling continuous and discrete event techniques, *Proceedings of the IFAC World Congress, Seoul, Korea*, pp. 7265–7270.

Benazera, E. and Travé-Massuyès, L. (2009). Set-theoretic estimation of hybrid system configurations, *IEEE Transactions on Systems, Man and Cybernetics, Part B: Cybernetics* **39**(5): 1277–1291.

Benazera, E., Travé-Massuyès, L. and Dague, P. (2002). State tracking of uncertain hybrid concurrent systems, *Proceedings of the 13th International Workshop on Principles of Diagnosis (DX02), Semmering, Austria*, pp. 106–114.

Blom, H. and Bar-Shalom, Y. (1988). The interacting multiple model algorithm for systems with Markovian switching coefficients, *IEEE Transactions on Automatic Control* **33**(8): 780–783.

Chow, E. and Willsky, A. (1984). Analytical redundancy and the design of robust failure detection systems, *IEEE Transactions on Automatic Control* **29**(7): 603–614.

Cocquempot, V., El Mezyani, T. and Staroswiecki, M. (2004). Fault detection and isolation for hybrid systems using structured parity residuals, *5th Asian Control Conference, Melbourne, Australia*, Vol. 2, pp. 1204 –1212.

Daigle, M., Roychoudhury, I., Biswas, G., Koutsoukos, X., Patterson-Hine, A. and Poll, S. (2010). A comprehensive diagnosis methodology for complex hybrid systems: A case study on spacecraft power distribution systems, *IEEE Transactions on Systems, Man, and Cybernetics, Part A: Systems and Humans* **4**(5): 917–931.

de Freitas, N. (2002). Rao–Blackwellised particle filtering for fault diagnosis, *Proceedings of the IEEE Aerospace Conference 2002, Big Sky, MT, USA*, Vol. 4, pp. 1767–1772.

Dearden, R. and Clancy, D. (2002). Particle filters for real-time fault detection in planetary rovers, *13th International Workshop on Principles of Diagnosis, DX02, Semmering, Austria*, pp. 1–6.

Georges, J.-P., Theilliol, D., Cocquempot, V., Ponsart, J.-C. and Aubrun, C. (2011). Fault tolerance in networked control systems under intermittent observations, *International Journal of Applied Mathematics and Computer Science* **21**(4): 639–648, DOI: 10.2478/v10006-011-0050-x.

Gertler, J. (1991). A survey of analytical redundancy methods in failure detection and isolation, *Preprints of the IFAC SAFEPROCESS Symposium, Baden-Baden, Germany*, pp. 9–21.

Henzinger, T. (1996). The theory of hybrid automata, *Proceedings of the 11th Annual IEEE Symposium on Logic in Computer Science (LICS '96), New Brunswick, NJ, USA*, pp. 278–292.

Hofbaur, M., Travé-Massuyès, L., Rienmüller, T. and Bayoudh, M. (2010). Overcoming non-discernibility through mode-sequence analytic redundancy relations in hybrid diagnosis and estimation, *21st International Workshop on Principles of Diagnosis DX-10, Portland, OR, USA*, pp. 71–78.

Hofbaur, M.W. (2005). *Hybrid Estimation of Complex Systems*, Lectures Notes in Control and Information Sciences, Vol. 319, Springer-Verlag, Berlin/Heidelberg/New York, NY.

Hofbaur, M.W. and Williams, B.C. (2002). Mode estimation of probabilistic hybrid systems, *in* C. Tomlin and M. Greenstreet (Eds.), *Hybrid Systems: Computation and Control, HSCC 2002*, Lecture Notes in Computer Science, Vol. 2289, Springer-Verlag, Berlin/Heidelberg, pp. 253–266.

Hofbaur, M.W. and Williams, B.C. (2004). Hybrid estimation of complex systems, *IEEE Transactions on Systems, Man, and Cybernetics, Part B: Cybernetics* **34**(5): 2178–2191.

Kamau, S. and Lunze, J. (2003). Controller synthesis for linear switched systems, *IFAC Conference on Analysis and Design of Hybrid Systems, Saint Malo, France*, pp. 141–146.

Koutsoukos, X., Kurien, J. and Zhao, F. (2002). Monitoring and diagnosis of hybrid systems using particle filtering methods, *15th International Symposium on Mathematical Theory Networks and Systems, South Bend, IN, USA* pp. 1–15.

Li, X. and Bar-Shalom, Y. (1996). Multiple-model estimation with variable structure, *IEEE Transactions on Automatic Control* **41**(4): 478–493.

Narasimhan, S. and Biswas, G. (2002). An approach to model-based diagnosis of hybrid systems, *in* C. Tomlin and M. Greenstreet (Eds.), *Hybrid Systems: Computation and Control, HSCC 2002*, Lecture Notes in Computer Science, Vol. 2289, Springer-Verlag, Berlin/Heidelberg, pp. 308–322.

Narasimhan, S., Dearden, R. and Benazera, E. (2004). Combining particle filters and consistency based approaches for monitoring and diagnosis of stochastic hybrid systems, *Proceedings of the 15th International Workshop on Principles of Diagnosis (DX04), Carcassonne, France*, pp. 123–128.

Olive, X. (2012). FDI(R) for satellites: How to deal with high availability and robustness in the space domain?, *International Journal of Applied Mathematics and Computer Science* **22**(1): 99–107, DOI: 10.2478/v10006-012-0007-8.

Rienmüller, T., Bayoudh, M., Hofbaur, M. and Travé-Massuyès, L. (2009). Hybrid estimation through synergic mode-set focusing, *IFAC SAFEPROCESS Symposium, Barcelona, Spain*, pp. 462–467.

Semerdjiev, E. and Mihaylova, L. (1998). Adaptive interacting multiple model algorithm for manoeuvring ship tracking, *1998 International Conference on Information Fusion, Las Vegas, NV, USA*, pp. 974–979.

Staroswiecki, M. and Comet-Varga, G. (2001). Analytical redundancy relations for fault detection and isolation in algebraic dynamic systems, *Automatica* **37**(5): 687–699.

Verma, V., Gordon, G., Simmons, R. and Thrun, S. (2004). Real-time fault diagnosis, *IEEE Robotics and Automation Magazine* **11**(2): 56–66.

Vidal, R., Chiuso, A., Soatto, S. and Sastry, S. (2003). Observability of linear hybrid systems, *Hybrid Systems: Computation and Control, HSCC 2003*, Lecture Notes in Computer Science, Vol. 2623, Springer-Verlag, Berlin/Heidelberg/New York, NY, pp. 526–539.

Theresa Rienmüller received her B.Sc. and M.Sc. degrees in telematics (computer sciences and electrical engineering) from the Graz University of Technology in 2005 and 2008, respectively. Her studies were focused on computer vision, telecommunications and mobile computing. Between January 2007 and December 2009, she was with the Institute of Control Engineering at the Graz University of Technology, Austria. From January 2010 to June 2010 she was a research assistant at the Institute of Automation and Control at UMIT, Hall in Tyrol, Austria. Currently she is a university assistant at the Institute of Electrical and Biomedical Engineering, UMIT. Her area of interest presently includes estimation and diagnosis of complex hybrid systems.

Michael Hofbaur is a full professor and chair of the Institute of Automation and Control Engineering at UMIT, Hall/Tyrol, Austria. He received his Dr.techn. from the Faculty of Electrical Engineering at the Graz University of Technology in 1999 and obtained the *venia docendi* at Graz for the scientific field of automation of complex systems in 2004. Before joining UMIT in 2009, he was with the Graz University of Technology (Institute of Control Engineering) and with MIT, Cambridge, USA (AI Lab and Space Systems Lab) as a visiting assistant professor (2000/2001). His research interests include model-based methods for estimation, diagnosis and control of complex hybrid systems, with applications in autonomous mobile and immobile robots.

Louise Travé-Massuyès is a research director of the National Centre for Scientific Research (CNRS), working at the Laboratory for Analysis and Architecture of Systems (LAAS), Toulouse, France, where she leads the Diagnosis and Supervisory Control (DISCO) Research Team. She received a Ph.D. degree in control in 1984 and an engineering degree, specializing in control, electronics and computer science in 1982, both from the National Institute of Applied Sciences (INSA) and then an *Habilitation á Diriger des Recherches* from Paul Sabatier University in 1998, all in Toulouse, France. Her main research interests are in qualitative and model-based reasoning as well as applications to dynamic systems supervision and diagnosis. She has been particularly active in bridging the AI and control model-based diagnosis communities, initially as the leader of the BRIDGE Task Group of the MONET European Network. She is a member of the IFAC Safeprocess Technical Committee and a senior member of the IEEE Computer Society.

Mehdi Bayoudh received his master degree in automatic control, computer science and industrial systems from the Electrotechnology, Electronics, Computer Science, Hydraulics and Telecommunications Engineering School (ENSEEIHT), Toulouse, with first-class honors in 2005, and a Ph.D. degree in embedded systems from the National Polytechnic Institute, Toulouse, in 2009. He also received the 2009 Léopold Escande award for the best Ph.D. In 2005–2009 he was a Ph.D. student at the LAAS-CNRS/Thales Alenia Space corporation, Toulouse/Cannes, Laboratory of Analysis and Systems Architecture. From 2009 to 2010 he was a research engineer at CNRS/CNES, Toulouse, within the AGATA program (Generic Architecture for Autonomy, Tests and Applications). Currently he is a computer science engineer at Amadeus, SAS, Sophia Antipolis, Cedex, France.

Appendix

Reference frames

First, let $S = (x, y, z)$ denote the satellite fixed frame, R the inertial (Galilean) frame and $C = (X, Y, Z)$ the target attitude frame (Fig. A1) that depends on the satellite mission.

We take the telecommunication convention. Hence the instantaneous rotation vector of the target attitude frame C relative to the inertial frame R expressed in

the target attitude frame is given by $\mathbf{\Omega}^{[C]}_{C/R} = -\omega_0 Y$, where ω_0 is the rotational velocity of the satellite about the Y-axis.

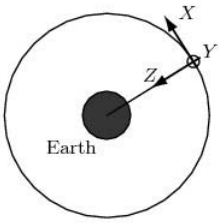

Fig. A1. Target attitude frame $C = (X, Y, Z)$ for a satellite.

The attitude control system aims to instantaneously place the satellite fixed frame S in the target frame C, i.e., to maintain the difference between these two frames, the smallest possible. Figure A2 depicts the *Cardan* angles $(\theta_L, \theta_T, \theta_R)$ that express the rotation between the two frames.

The rotation vector of the satellite fixed frame S relative to the target attitude frame C, expressed in S, is given by (xyz-convention)

$$\mathbf{\Omega}^{[S]}_{S/C} = \begin{bmatrix} \dot\theta_R - \dot\theta_L \sin\theta_T \\ \dot\theta_T \cos\theta_R + \dot\theta_L \cos\theta_T \sin\theta_R \\ \dot\theta_L \cos\theta_T \cos\theta_R - \dot\theta_T \sin\theta_R \end{bmatrix}. \qquad \text{(A1)}$$

Since the difference between the satellite fixed frame S and the target frame C is very small, we can take the approximation of small angles and obtain the rotation vector of the satellite fixed frame S relative to the target attitude frame C, expressed in the satellite fixed frame

$$\mathbf{\Omega}^{[S]}_{S/C} \approx \begin{bmatrix} \dot\theta_R \\ \dot\theta_T \\ \dot\theta_L \end{bmatrix},$$

and the rotation matrix of the frame S relative to the frame C

$$\mathbf{M}_{S\to C} \approx \begin{bmatrix} 1 & \theta_L & -\theta_T \\ -\theta_L & 1 & \theta_R \\ \theta_T & -\theta_R & 1 \end{bmatrix}.$$

The rotation vector of the target attitude frame C relative to the inertial frame R, expressed in the satellite fixed frame S, is given by

$$\begin{aligned} \mathbf{\Omega}^{[S]}_{C/R} &= \mathbf{M}_{S\to C}.\mathbf{\Omega}^{[C]}_{C/R} \\ &= \begin{bmatrix} 1 & \theta_L & -\theta_T \\ -\theta_L & 1 & \theta_R \\ \theta_T & -\theta_R & 1 \end{bmatrix} . \begin{bmatrix} 0 \\ -\omega_0 \\ 0 \end{bmatrix} \\ &= \begin{bmatrix} -\omega_0\theta_L \\ -\omega_0 \\ \omega_0\theta_R \end{bmatrix}. \end{aligned}$$

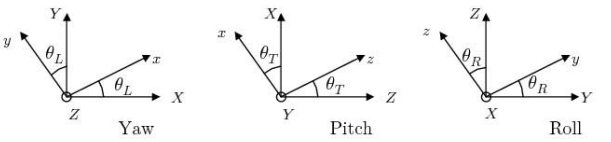

Fig. A2. Frame change using the Cardan angles $(\theta_L, \theta_T, \theta_R)$.

Finally, the rotation vector of the satellite fixed frame S relative to the inertial frame R, expressed in the satellite fixed frame S, is obtained by

$$\mathbf{\Omega}^{[S]}_{S/R} = \mathbf{\Omega}^{[S]}_{S/C} + \mathbf{\Omega}^{[S]}_{C/R} = \begin{bmatrix} \dot\theta_R - \omega_0\theta_L \\ \dot\theta_T - \omega_0 \\ \dot\theta_L + \omega_0\theta_R \end{bmatrix}.$$

Satellite dynamics. Let G denote the satellite's center of mass. We obtain for the time derivative of the satellite's angular momentum ($\mathbf{H}^{[S]}_G$) with respect to the inertial frame

$$\frac{\mathrm{d}}{\mathrm{d}t}_{/R}[\mathbf{H}^{[S]}_G] = \frac{\mathrm{d}}{\mathrm{d}t}_{/S}[\mathbf{H}^{[S]}_G] + \mathbf{\Omega}^{[S]}_{S/R} \times \mathbf{H}^{[S]}_G = \mathbf{M}^{[S]}_{F_{\text{ext}}}, \qquad \text{(A2)}$$

where $\mathbf{H}^{[S]}_G = \mathbf{I}_G \mathbf{\Omega}^{[S]}_{S/R}$ and

$$\mathbf{M}^{[S]}_{F_{ext}} = \begin{bmatrix} C_X \\ C_Y \\ C_Z \end{bmatrix}$$

denotes the momentum of external forces exerted on the satellite (torque). With the satellite inertia

$$\mathbf{I}_G = \begin{bmatrix} I_X & 0 & 0 \\ 0 & I_Y & 0 \\ 0 & 0 & I_Z \end{bmatrix},$$

Eqn. (A2) becomes (A3).

Applying the first order approximation, we finally obtain for the satellite dynamics

$$\begin{bmatrix} I_X(\ddot\theta_R - \omega_0\dot\theta_L) \\ I_Y\ddot\theta_T \\ I_Z(\ddot\theta_L + \omega_0\dot\theta_R) \end{bmatrix} + \begin{bmatrix} (I_Y - I_Z)\omega_0\dot\theta_L \\ 0 \\ (I_X - I_Y)\omega_0\dot\theta_R \end{bmatrix} = \begin{bmatrix} C_X \\ C_Y \\ C_Z \end{bmatrix}. \qquad \text{(A4)}$$

Actuators. In this case study, we assume that the attitude control is achieved by three reaction wheels placed in the satellite axes: X, Y and Z.

The torque provided by a wheel is given by

$$\mathbf{C}_{\text{wheel}} = -\mathbf{\Omega}^{[S]}_{S/R} \times \mathbf{H}^{[S]}_{\text{wheel}} - \frac{\mathrm{d}}{\mathrm{d}t}_{/S}[\mathbf{H}^{[S]}_{\text{wheel}}], \qquad \text{(A5)}$$

where $\mathbf{H}^{[S]}_{\text{wheel}}$ denotes the angular momentum of the wheel.

$$\begin{bmatrix} C_X \\ C_Y \\ C_Z \end{bmatrix} = \begin{bmatrix} I_X(\ddot{\theta}_R - \omega_0\dot{\theta}_L) \\ I_Y\ddot{\theta}_T \\ I_Z(\ddot{\theta}_L + \omega_0\dot{\theta}_R) \end{bmatrix} + \begin{bmatrix} (\dot{\theta}_T - \omega_0)I_Z(\dot{\theta}_L + \omega_0\theta_R) - (\dot{\theta}_L + \omega_0\theta_R)I_Y(\dot{\theta}_T - \omega_0) \\ -(\dot{\theta}_R - \omega_0\theta_L)I_Z(\dot{\theta}_L + \omega_0\theta_R) + (\dot{\theta}_L + \omega_0\theta_R)I_X(\dot{\theta}_R - \omega_0\theta_L) \\ (\dot{\theta}_R - \omega_0\theta_L)I_Y(\dot{\theta}_T - \omega_0) - (\dot{\theta}_T - \omega_0)I_X(\dot{\theta}_R - \omega_0\theta_L) \end{bmatrix} \quad \text{(A3)}$$

The first term is negligible in the case of a reaction wheel, since the wheel velocity is small and the torque is provided by a variation in the wheel velocity.

The angular momentum of all three reaction wheels becomes

$$\mathbf{H}^{[S]}_{\text{wheels}} = I_W \begin{bmatrix} \dot{\theta}_X \\ \dot{\theta}_Y \\ \dot{\theta}_Z \end{bmatrix}, \quad \text{(A6)}$$

where $\dot{\theta}_X, \dot{\theta}_Y$ and $\dot{\theta}_Z$ are the rotation velocity of the reaction wheels placed in X, Y and Z axes, respectively, and I_W is the wheel inertia.

The torque exerted on the satellite is given by

$$\mathbf{C} \approx -\frac{\mathrm{d}}{\mathrm{d}t}_{/S}[\mathbf{H}^{[S]}_{\text{wheel}}] = \begin{bmatrix} -I_W\ddot{\theta}_X \\ -I_W\ddot{\theta}_Y \\ -I_W\ddot{\theta}_Z. \end{bmatrix}. \quad \text{(A7)}$$

Each wheel is composed of a flywheel and a rotating motor that provides torque by accelerating the wheel rotation. When the wheel velocity reaches the maximum velocity, other kinds of actuators (e.g., thrusters) are used to de-saturate the wheel[6].

Sensors. We use gyro-meters that measure the rotation vector of the satellite fixed frame S relative to the inertial frame R:

$$\mathbf{\Omega}^{[S]}_{S/R} = \begin{bmatrix} p \\ q \\ r \end{bmatrix} = \begin{bmatrix} \dot{\theta}_R - \omega_0\theta_L \\ \dot{\theta}_T - \omega_0 \\ \dot{\theta}_L + \omega_0\theta_R \end{bmatrix}.$$

Received: 14 November 2011
Revised: 10 May 2012

[6]The de-saturation is achieved by thrusters exerting torque that decreases the rotation velocity of the wheel.